Exohedral Physisorption of Ambient Moisture Scales Non-monotonically with Fiber Proximity in Aligned Carbon Nanotube Arrays

Itai Y. Stein

Department of Mechanical Engineering, Massachusetts Institute of Technology,
77 Massachusetts Ave, Cambridge, MA 02139, USA.

Noa Lachman and Brian L. Wardle*

Department of Aeronautics and Astronautics, Massachusetts Institute of Technology,
77 Massachusetts Ave, Cambridge, MA 02139, USA.

Mackenzie E. Devoe

Department of Materials Science and Engineering, Massachusetts Institute of Technology,
77 Massachusetts Ave, Cambridge, MA 02139, USA.

Here we present a study on the presence of physisorbed water on the surface of aligned carbon nanotubes (CNTs) in ambient conditions, where the wet CNT array mass can be more than 200% larger than that of dry CNTs, and modeling indicates that a water layer > 5 nm thick can be present on the outer CNT surface. The experimentally observed non-linear and non-monotonic dependence of the mass of adsorbed water on the CNT packing (volume fraction) originates from two competing modes. Physisorbed water cannot be neglected in the design and fabrication of materials and devices using nanowires/nanofibers, especially CNTs, and further experimental and *ab initio* studies on the influence of defects on the surface energies of CNTs, and nanowires/nanofibers in general, are necessary to understand the underlying physics and chemistry that govern this system.

One dimensional nanoscale systems, such as nanowires, nanofibers, and nanotubes, are well known for their phenomenal electrical,[1–4] thermal,[5–8] and mechanical properties,[9–11] which could enable the design and manufacture of next-generation materials with unprecedented properties.[12–18] However, while many studies have previously explored the synthesis of new architectures and devices using one dimensional nanomaterials, specifically carbon nanotubes (CNTs), the properties they reported were far lower than the properties of predicted using current theory.[12] Some of the main reasons why existing models cannot accurately predict the behavior of CNTs in scalable architectures, such as aligned CNT arrays, are the various CNT morphology and proximity effects,[13–15, 19] which can strongly impact properties, but are not well understood and cannot be properly integrated into theoretical frameworks. Here we report the presence of a commonly neglected morphological effect, an unexpectedly large (compared to the CNT mass) amount of moisture located on the surface of CNTs in aligned CNT (A-CNT) arrays at ambient conditions; show the non-linear and non-monotonic dependence of this effect on array porosity, which suggests two competing mechanisms; and discuss the strong impact such an effect can have on the structure and properties of nanocomposite architectures composed of A-CNTs.

Previous studies on how water interacts with the outer surface of a CNT illustrated that the water molecules form a layer-like shell surrounding the CNTs,[20–23] and that the water layer density varies greatly and non-monotonically with its thickness.[21, 22] A recent study on the physisorption of water onto the external surface of a suspended $\sim 1.1 - 1.2$ nm diameter single walled CNT showed that more than one layer of water is present on the CNT surface in water vapor, and that water molecules more easily adsorb onto larger diameter CNTs.[24] However, this study was limited to isolated and defect-free CNTs,[24, 25] meaning that the interaction of moisture present in ambient air with multiwalled CNTs, which normally have native wall defects,[26] in aligned arrays is currently unknown. Here we show that depending on the inter-CNT spacing, the amount of water that is physisorbed onto the CNT surface in the arrays is governed by competing mechanisms that are a function of CNT proximity. The implications of the physisorbed water on the A-CNT arrays are two-fold: 1) the behavior of the CNT array as a whole may be altered, due to a change in electrostatic interactions between the individual CNTs; 2) adsorbed water can alter the intrinsic properties of the CNTs, and can hinder the deposition of a secondary material onto the CNT surface with implications for processing. Sensitivity of CNT devices to moisture was previously reported in a number of studies,[13] yet the exact mechanism of water interference is still debated, and is one of the primary challenges of designing and operating CNT architectures at ambient conditions.[13] In this report, some of the electrostatic effects that could be responsible for the origin of the physisorbed water layer are discussed, and future work that could enable better understanding, and ultimately control, of the moisture sensitivity of CNT architectures is proposed.
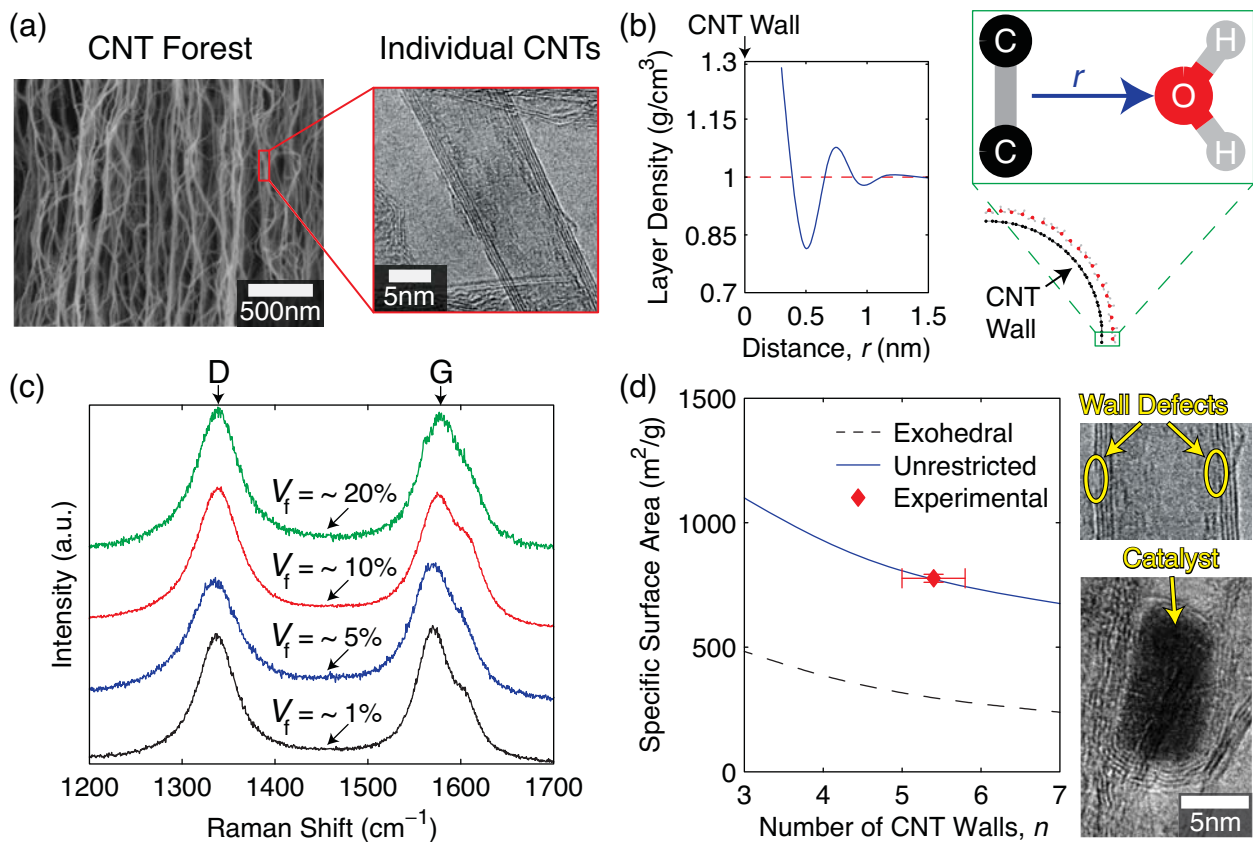
---

* wardle@mit.edu.

FIG. 1. (a) HRSEM image showing the morphology of an as-grown CNT forest and HRTEM image showing the structure of individual CNTs that make up the forest. (b) Plot of the layer density profile of water physisorbed onto the surface of a CNT from a previously reported MD simulation illustrating the strong influence of film thickness for thin ($\lesssim 1$ nm) films of physisorbed water.[21] (c) Raman spectra illustrating that the CNTs used in this study had a significant number of defects (I_G/I_D ratios $\lesssim 1$). (d) plot of the specific surface area as a function of number of CNT walls for CNTs with no wall defects (exohedral adsorption) and with wall defects (unrestricted adsorption), and HRTEM images showing that the multiwalled CNTs used here are capped and have a significant number of wall defects.

RESULTS

CNT surface structure and interaction with adsorbates

Since electrostatic interactions are heavily dependent on the exposed surface of the material, the surface morphology of the CNTs was characterized using both scanning (SEM) and transmission (TEM) electron microscopy (see Figure 1a). In order to quantify the amount of water present on the CNT surface, the influence of the CNT surface on the molecular orientation and moisture layer density was examined using the results of previously reported molecular dynamics (MD) simulations.[20–22] These simulations illustrate that at layer thicknesses below 1 nm, water molecules interacting with the outside surface (known as the exohedral surface) of the CNT have preferred orientations, and assume a spatially varying density profile (see Figure 1b) that is independent of CNT outer diameter.[21, 22] On the other hand, these simulations show that water molecules interacting with

the inside surface (known as the endohedral surface) are strongly influenced by confinement effects,[27–29] and assume density profiles that are a strong function of the CNT inner diameter.[20, 21, 30] While the scaling behavior of the water layer density observed in these simulations should be similar for CNTs with native wall defects (such as those ones used here), differences in interaction potentials mean that the results of these previous studies may not be representative of the current system of aligned CNTs. Another consequence of confinement effects is the formation of water clusters, which play a significant role in the stabilization of water in hydrophobic carbon micro and mesopores.[31, 32] By forming clusters of 5 or more water molecules (cluster size of ~ 1 nm),[31, 33–35] the affinity of the water molecules can be transformed from hydrophillic to hydrophobic,[33] making their interaction with the CNT walls more favorable. While many previous studies have explored the mechanics, kinetics, and energetics of the entry of water molecules into uncapped single walled CNTs,[30, 36–38] the likelihood that a water molecule can enter the

inner region of a capped multiwalled CNT *via* wall defects is low (since the openings in the CNT walls are likely smaller than the cluster size), meaning that the exohedral physisorption of water is expected. Wall defects may also lead to the following: higher CNT surface energies[39], which lead to stronger interactions with water molecules[40, 41] and enable the separation of salt ions from solution[42]; altered electronic properties,[43–46] which can lead to a CNT behaving as either a metal or semi-conductor,[43] and can also lead to reversible wetting and de-wetting of water in nanopores.[47] Since wall defects can fundamentally change the CNT-water interactions,[48] their characterization is necessary.

Defect concentration is evaluated *via* the Raman spectra of the CNTs with volume fractions, defined as V_f, up to 20% (see Figure 1c). The resulting ratios of the integrated intensities of the G and D peaks, known as the I_G/I_D ratio, illustrate that the defect concentration in the CNTs was non-negligible, since the evaluated I_G/I_D values for all values of V_f were $\lesssim 1$ and not $\gg 1$, the expected I_G/I_D for largely defect free graphitic carbon systems.[26, 49, 50] Such wall defects are well-known in multiwalled CNTs synthesized *via* chemical vapor deposition.[51] While Raman spectroscopy is a very useful tool for studying defects in carbon materials,[52] the quantitative study of wall defects in multiwalled CNTs using Raman scattering is very challenging,[26] so a secondary technique was therefore utilized: evaluation of the specific surface area of the CNTs using the adsorption isotherms of Kr *via* the theory developed by Brunauer, Emmett, and Teller (known as BET).[53] Figure 1d shows that the experimentally determined specific surface area of the CNTs is $(776.8 \pm 16.3 \text{ m}^2/\text{g})$, a value consistent with a monolayer of Kr adsorbing onto both the exohedral and endohedral surfaces of the CNTs, defined as unrestricted adsorption.[54] The equations used to compute the specific surface area of CNTs undergoing both exohedral and unrestricted adsorption and a table of the model predicted specific surface areas as a function of the number of CNT walls can be found in the Supporting Information. Since these CNTs are capped (see Figure 1d for an HRTEM image of a CNT attached to a catalyst particle), unrestricted adsorption could only occur if wall defects such as ultra-micropores (< 0.7 nm in diameter) or interlayer bonds are present. See Figure 1d for an HRTEM image that shows an example of a CNT with wall defects.

Theoretical framework

Since electrostatic effects have a very strong dependence on CNT separation distance, a theoretical framework that describes the inter-CNT spacing as a function V_f was necessary. This was achieved using a previously developed continuous coordination model for the average inter-nanowire (NW) spacing (Γ) of aligned NW arrays.[55] The origin of Γ as a function of the two di-

mensional coordination number (N) is further discussed in the Supporting Information. Since the previous study used HRSEM, a method which is only accurate in one dimension (depth information is lost), to approximate the inter-CNT spacing, the minimum ($\Gamma_{\min}$) and maximum ($\Gamma_{\max}$) values of the inter-CNT spacing evaluated for each coordination (see Figure S1 in the Supporting Information) were assumed to have equal contribution and were combined into a 1D average, previously defined as Γ. However, since the scaling behavior of the electrostatic effects in defective CNTs is not currently known, the assumption that $\Gamma_{\min}$ and $\Gamma_{\max}$ contribute equally is not justified, and their independent evaluation is therefore necessary. See Figure 2a for a plot of Γ, $\Gamma_{\min}$, and $\Gamma_{\max}$ as a function of V_f (the equations of Γ, $\Gamma_{\min}$, and $\Gamma_{\max}$ can be found in the Supporting Information).

Since previously reported MD simulations have shown that water molecules form a layer-like structure when interacting with the surface of a CNT,[20–24] the physisorbed water molecules are modeled as a layer which adheres to the previously reported density profile (see Figure 1b).[21] As illustrated by Figure 1d, the wall defects of the CNTs allow for unrestricted adsorption of Kr molecules, but since water molecules require large openings ($\gtrsim 0.6$ nm due to an equilibrium water-CNT wall separation of ~ 0.3 nm[21]) to access the internal region of the CNT, the adsorption of the water molecules is taken as only exohedral in nature (see Figure 2b for an illustration of the model geometry). This assumption is revisited in the next subsection.

Using these assumptions, two easily accessible physical measures of the CNT arrays can be evaluated as a function of the thickness of the water layer (w): the ratio of wet and dry mass of the CNT array ($m^\star$); and CNT array porosity unoccupied by water, defined as accessible porosity (ϕ). w can be determined using the following geometric relation involving $m^\star$; the inner (D_i) and outer (D_o) diameters of the CNTs (a previous HRTEM study showed that these CNTs are comprised of 3 to 7 walls with average $D_i \simeq 5$ nm and $D_o \simeq 8$ nm);[56] the ratio of the CNT intrinsic density ($\rho_{cnt} \to \simeq 1.7$ g/cm^3)[57] and the average density of the water layer (ρ_w); and the equilibrium separation of the water molecules and the CNT wall ($\ell \to \simeq 0.3$ nm)[21]:

$$w = \left(\sqrt{(D_o^2 - D_i^2)\left(\frac{\rho_{cnt}}{\rho_w}(m^\star - 1)\right) - D_i^2} \right) - D_o + \ell \tag{1}$$

The procedure used to evaluate eq 1 can be found in the Supporting Information. To find ϕ, the amount of inter-CNT space not occupied by water needs to be evaluated. This can be done using the isosceles angle of the constitutive triangles at each coordination (θ) and $\Gamma_{\min}$ (details can be found in the Supporting Information), and yields the following relationship:

$$\phi = 1 - \frac{\pi}{8\tan(\theta)}\left(\frac{D_o + 2w}{2\cos(\theta)\left(\Gamma_{min} + \frac{D_o}{1+2\cos(\theta)}\right)}\right)^2 \quad (2)$$

As eq 2 demonstrates, ϕ is a very strong function of Γ_{min}, meaning that ϕ for as-grown A-CNTs ($V_f \sim 1\% \to \Gamma_{min} \sim 60$ nm) is largely unaffected by the presence of physisorbed water, whereas densified A-CNTs with $V_f \gtrsim 5\%$ ($\to \Gamma_{min} \lesssim 20$ nm) may have a ϕ of 60% or less. See Figure 2c for a plot of ϕ as a function of Γ_{min}.

Water physisorption as a function of volume fraction

Using the ratio of the wet and dry mass of the CNT arrays ($m^\star$), eq 1 was used to evaluate the thickness of the exohedral water (w) present on the CNT surface in ambient conditions. See Table S3 in the Supporting Information for the experimentally determined wet and dry CNT array mass ratios and the evaluated w values. No changes in A-CNT volumes were observed since the water layer thicknesses ($\sim 3 - 5$ nm) are smaller than the minimum inter-CNT separations ($\sim 10 - 60$ nm). The trend of water layer thickness (see Figure 3a), which increases from $V_f = 1\%$ to $V_f = 5\%$ and then decreases from $V_f = 5\%$ to $V_f = 20\%$, demonstrates that at least two competing modes are present with a crossover point at $V_f = \sim 5\%$. To simplify the analysis, two competing modes were defined: Mode I ($1\% \gtrsim V_f \gtrsim 5\%$); and Mode II ($5\% \gtrsim V_f \gtrsim 20\%$). To evaluate the scaling behavior of each mode, the non-dimensional reduced thickness of the water layer, defined as the ratio of w and $0.5\Gamma_{min}$, was plotted as a function V_f (see Figure S2 in the Supporting Information), and each regime was fit with a straight line with coefficients of determination (R^2) $\gtrsim 0.98$. As Figure 3a illustrates, the predicted crossover point of the two modes occurs at $V_f \sim 5.3\%$, when the separation of the exohedral water layers is ~ 10 nm ($\Gamma_{min} \sim 24$ nm and $w \sim 7$ nm), which is where retardation effects can begin to influence the interactions of NWs.[58] The implications of these retardation effects is discussed further in the Discussion.

Since the physisorbed water layer might hinder the adherence of a second material onto the CNT surface, especially hydrophobic materials such as polymers, the experimentally determined infusion efficacy of the A-CNT arrays with a hydrophobic phenolic resin were used to estimate the accessible array porosity (ϕ) as a function of V_f. See Table S3 in the Supporting Information for the experimentally determined ϕ values for the polymer infusion study, and Figure S2 for cross-sectional SEM micrographs of as-grown (Figure S2a) and densified A-CNTs (Figure S2b) and a densified A-CNT polymer nanocomposite (Figure S2c) illustrating continuous through thickness infusion with polymer even for A-CNTs with $V_f \sim 20\%$ (Figure S2c). The resulting ex-
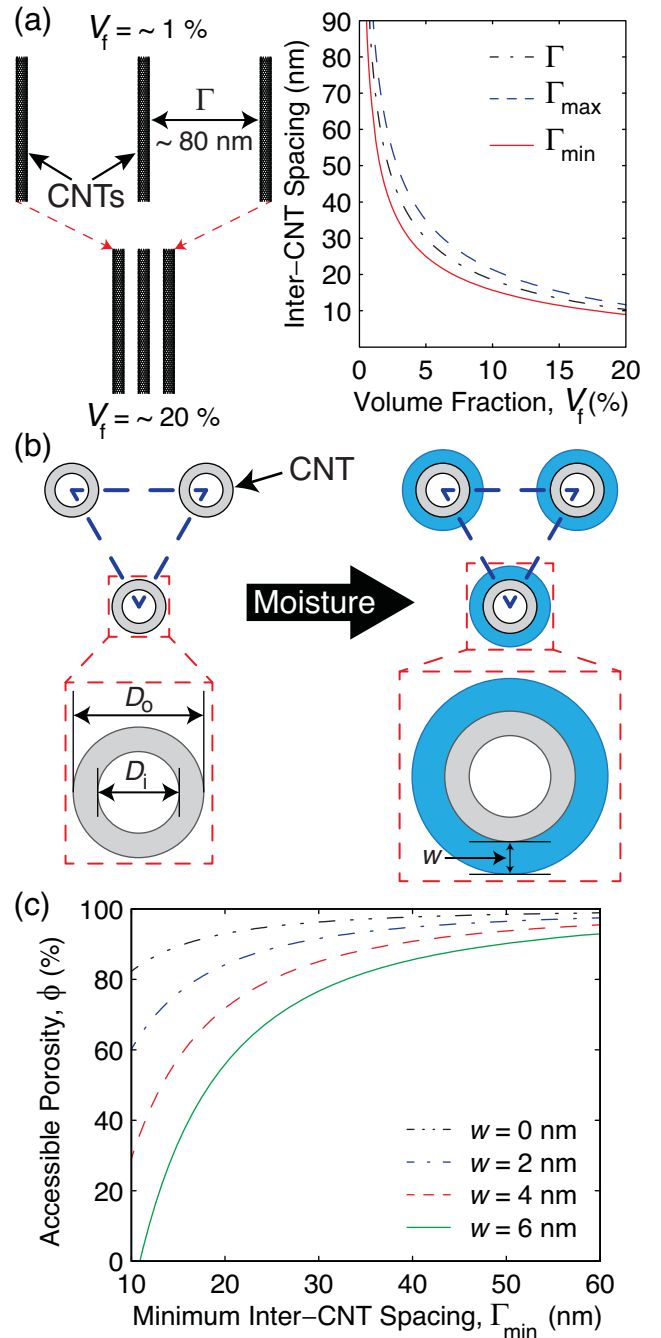

FIG. 2. (a) Geometry and results of the inter-CNT spacing analysis performed using a previously reported continuous coordination model[55]. (b) Geometry used to model the exohedral layer-like physisorption of water molecules on the CNTs in the forests. (c) Plot of the available porosity as a function of minimum inter-CNT spacing for water layers up to 6 nm thick.

perimentally determined estimates of the accessible array porosity were then compared to the ones predicted by eq 2 using the w values evaluated *via* eq 1 (see Figure 3b). As Figure 3b illustrates, both measurements show good agreement, and that the presence of the physisorbed wa-
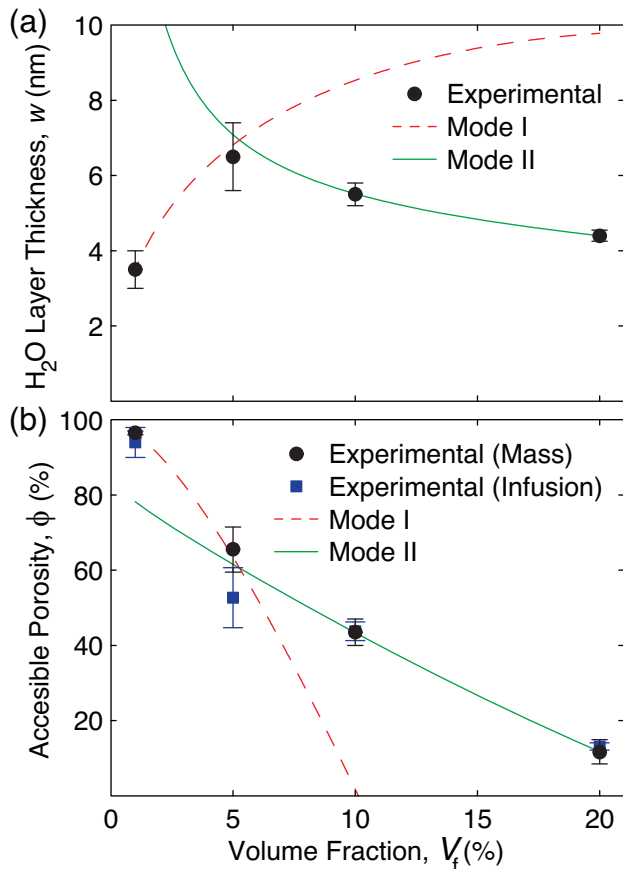
FIG. 3. (a) Water layer thickness (w) as a function of CNT volume fraction (V_f) showing the non-linear and non-monotonic dependence of the physisorption process on CNT proximity and indicating a change of mechanism at $V_f \sim 5.3\%$. (b) Plot of the accessible porosity of the CNT arrays evaluated using the ratio of the dry and wet CNT array mass (see eq 2 and Table S3 in the Supporting Information) and infusion of the CNT arrays with a hydrophobic phenolic resin. The plot illustrates the strong influence of the thickness of the physisorbed water layer, especially at $V_f \gtrsim 5\%$.

ter layer becomes very significant at $V_f \gtrsim 5\%$. An important note should be made about the large uncertainties of the data points at $V_f \sim 5\%$, which did not allow the experimental evaluation of the crossover point of Modes I and II using the current densification technique with sufficient confidence. The origin of the experimental uncertainty is discussed further in the next section.

DISCUSSION

Since the Raman spectras exhibit $I_G/I_D \lesssim 1$, and the specific surface areas evaluated using the BET analysis[53] show that Kr can adsorb onto both the exohedral and endohedral surfaces of the CNTs, a non-negligible amount of wall defects are likely present in the CNTs used in this study. These results are consistent with a recent study on the adsorption of CO_2 onto double walled CNTs, where the predicted specific surface area was slightly ($\sim 10\%$) lower than the experimentally determine one, indicating that unrestricted physisorption took place.[54] However, for the case of water physisorption, the accessible porosity results presented here (see Figure 3b) indicate that the water molecules do not penetrate the inner CNT volumes to a significant degree, meaning that the adsorption was exohedral in nature. This is likely a result of the size and morphology of wall defects, which are smaller than the size of the water clusters (~ 1 nm) that enable the physisorption of water onto the CNT walls.[31, 33–35] Recent work on graphite indicates that lattice monovacancies can become mobile at temperatures $\gtrsim 200°C$,[59] and that the aggregation of these vacancies can lead to the formation of interlayer bonds, known as interlayer divacancies,[59–61] which can become the nucleation site for an extended interlayer defect, where two CNT wall planes become connected via a graphene ribbon.[60] The aggregation of native CNT wall defects likely do not provide continuous through-thickness pathways of sufficient size ($\gtrsim 0.6$ nm) to enable the water clusters to enter the inner volume of the CNTs. Further work is necessary to determine the size and morphology of the native wall defects present in the CNTs used here, and the effect of the CNT structure and surface chemistry on the kinetics and energetics of the exohedral physisorption of water.

The amount of adsorbed water is significantly larger than the recently reported value for isolated single walled CNTs,[24] and the water layer thickness varies non-linearly and non-monotonically with CNT proximity. The V_f dependence can be explained by considering two competing modes analogous to the pairwise potential commonly used to simulate atomic interactions[62, 63]: Mode I, which represents long range attractive interactions; and Mode II, which represents short range repulsive interactions. Of interest is the crossover point of the two modes, which occurs at $V_f \sim 5.3\%$ where $\Gamma_{min} \sim 24$ nm. Electrostatic forces, which originate from quantum fluctuations in the electromagnetic field, play a significant role in the interaction of nanostructures, molecules, and surfaces with nm-scale separations.[64–66] In small separations ($\lesssim$ a few nanometers),[65] known as the non-retarded regime, these forces are commonly known as the van der Waals forces.[64, 65] However, in larger separations a virtual photon emitted from one nanostructure may not be able to reach, and therefore be absorbed, by another nanostructure during its lifetime (as determined by the Heisenberg uncertainty).[65] This regime is known as the relativistic retarded regime,[65] where the finite speed of light leads to significant attenuation of the dispersion interactions,[64] and the resulting fluctuations in dipole moments lead to forces known as the Casimir forces.[65, 67] Recent studies on the interactions of two materials, including NWs, separated by a thin film of fluid have shown that the Casimir[68, 69] interaction energies can be either repulsive or attractive depending on

the permittivities of the materials (NWs and fluids).[70–72] They also reported that, due to retardation effects, the separation of the two materials has a very strong influence on the permittivities,[71] which could transform the Casimir interaction energy from attractive to repulsive at intermediate separations ($\lesssim 10$ nm).[72] This means that Mode I and Mode II may not be due to van der Waals interactions, which are usually dominant at relatively short separations,[58, 71–73] and may actually originate from the Casimir interactions that become significant at intermediate separations.[72] The presence of wall defects, which strongly influence the electronic properties of the CNTs (*e.g.* the dielectric permittivities),[43–46, 74] may also contribute to the presence of Casimir interactions, which were previously shown to influence adsorption on CNTs.[65, 75] The energetic and structural origin of the two modes observed here have yet to be elucidated. Recent studies on graphitic surfaces indicate that their affinity can change from hydrophobic to hydrophillic within minutes of exposure to ambient due to adsorption of volatile hydrocarbon species in ambient air.[76] Future work should explore the presence of hydrocarbon species on the CNT surface in ambient conditions, and the influence of defects, which are known to act as nucleation hotspots,[39, 77, 78] on the kinetics and energetics of hydrocarbon adsorption on CNTs.

The accessible porosity results (see Figure 3b) show that the physisorbed water can hinder the introduction of a coating or intermediate material into the CNT array, and will therefore impact the fabrication and performance of CNT-based devices. Since the biaxial densification technique used to control the V_f can lead to spatial inhomogeneities in V_f at low ($\lesssim 10\times$) densifications, the infusion results at $V_f \sim 5\%$ were associated with large uncertainties in local Γ_{min}. These uncertainties in Γ_{min} at $V_f \sim 5\%$ were estimated at $\sim \pm 10 - 15\%$, which lead to about the same order of magnitude of uncertainty in accessible porosity (see Figure 2c), as observed in the experimental data (see Figure 3b). Also, because previous studies on the capillary-assisted wetting of CNT arrays of varying V_f with epoxy resins, which are less sensitive to moisture than phenolics, did not observe such an impact on infusion yield,[79–82] further studies on the interaction of the physisorbed water layers with introduced polymer species of varying chemistries is necessary.

CONCLUSION

In conclusion, the presence of a non-negligible amount (on the order of the CNT array mass) of physisorbed water on the surface of CNTs in aligned arrays at ambient conditions was reported. The experimental results, coupled with theory, illustrate that the thickness of the physisorbed water layer present on the outer CNT surface scales non-monotonically with the CNT volume fraction (V_f), and ranges from ~ 3 nm to ~ 7 nm at $1\% \lesssim V_f \lesssim 20\%$. The non-monotonic V_f scaling be-havior of the water layer is attributed to two competing electrostatic modes that have a crossover point of ~ 25 nm inter-CNT spacing ($V_f \simeq 5.3\%$). Since a significant amount of wall defects was present in the CNTs used here, but their exact contribution to inter-CNT electrostatic interactions is not currently known, further study on the impact of wall defects on the surface energies of multiwalled CNTs is required. Once the mechanism in which wall defects influence the surface energies of CNTs is better understood, control over inter-CNT electrostatic interactions may become possible, allowing the design and manufacture of next-generation CNT architectures with tuned properties, such as insensitivity to moisture, allowing operation in ambient conditions,[13] or selective attraction of charged species (particles or ions), enabling low energy high throughput water purification.[42]

METHODS

Sample preparation

The A-CNT arrays were grown in a 22 mm internal diameter quartz tube furnace at atmospheric pressure *via* a previously described thermal catalytic chemical vapor deposition process using ethylene as the carbon source.[55, 79–81] The CNTs were grown on 1 cm × 1 cm Si substrates forming A-CNT arrays that are up to ~ 1 mm tall, and are composed of multiwalled CNTs that have an average outer diameter of ~ 8 nm ($3 - 7$ walls with an inner diameter of ~ 5 nm and intrinsic CNT density of ~ 1.7 g/cm^3),[56, 57] inter-CNT spacing of ~ 80 nm,[55] and V_f of $\sim 1\%$ CNTs.[56] The A-CNT arrays were then delaminated from the Si substrate using a standard lab razor blade, and mechanically densified (biaxially) to the desired V_f (up to $\sim 20\%$).[15, 55]

Surface morphology and wall defect characterization

The surface morphology of the CNTs was characterized using both scanning (SEM) and transmission (TEM) electron microscopy. The SEM analysis was performed using a JEOL 6700 cold field-emission gun SEM using secondary electron imaging at an accelerating voltage ranging from 1.0 (V_f up to 5% CNTs) to 1.5 kV ($V_f > 5\%$ CNTs) and a working distance of 3.0 mm.[55] The TEM analysis was performed using a JEOL 2100 TEM at an accelerating voltage of 120 kV.

Native wall defects present in the CNTs were characterized using both Raman spectroscopy and the Brunaur-Emmett-Teller (BET) surface area measurement. Raman spectra were collected using a LabRam HR800 Raman microscope (Horiba Jobin Yvon) with 532 nm (2.33 eV) laser excitation through a 50× objective (N.A. 0.75). The BET surface area measurement was performed using a Micromeritics ASAP 2020 Physisorption Analyzer and consisted of two stages: degas and analysis. Degas

consisted of two phases: evacuation and heating. The evacuation phase had the following parameters: temperature ramp rate of $10°C/min$; target temperature of $50°C$; evacuation rate of 5 mmHg/s; unrestricted evacuation from 5 mmHg; vacuum set point of 20 μmHg; evacuation time of 60 min. The heating phase used the following parameters: temperature ramp rate of $10°C/min$; hold temperature of $300°C$; hold time of 24 hours. Both degas phases had a hold pressure of 100 mmHg. The BET analysis was then performed using Kr, due to the low total surface area (< 10 m^2) of the A-CNTs. Additional details can be found elsewhere.[83]

Mass and array porosity quantification

The A-CNTs were dried using the degas conditions *via* a Micromeritics ASAP 2020 Physisorption Analyzer, and their dry mass was measured using a Mettler AE100 Analytical Balance. Previous work indicates that exposure to ambient conditions should result in CNTs with accessible porosity that is filled/nearly filled with water,[84] so the A-CNTs were exposed to ambient until their mass stabilized ($\sim$ 72 hrs). Once the mass of the A-CNTs stabilized, testing at different relative humidities indicated that the total amount of adsorbed water is not very sensitive ($\ll 5\%$ change) to the relative humidity of the ambient. The wet mass of the A-CNTs was then measured using a TA Instruments Discovery Thermogravimetric Analyzer. The accessible porosity of the CNT arrays was estimated by comparing the dry density of the pyrolytic carbon matrix of aligned CNT carbon matrix nanocomposites (V_f up to 20% CNTs), made *via* the pyrolysis of polymer matrix precursors,[57] with the dry density of pure pyrolytic carbon baseline samples. Additional details can be found elsewhere.[83]

[1] A. Bezryadin, C. N. Lau, and M. Tinkham, Nature **404**, 971 (2000).

[2] J. E. Mooij and Y. Nazarov, Nat. Phys. **2**, 169 (2006).

[3] J. Wang, M. Singh, M. Tian, N. Kumar, B. Liu, C. Shi, J. K. Jain, N. Samarth, T. E. Mallouk, and M. H. W. Chan, Nat. Phys. **6**, 389 (2010).

[4] K. Xu and J. R. Heath, Nano Lett. **8**, 3845 (2008).

[5] S. Shen, A. Henry, J. Tong, R. Zheng, and G. Chen, Nat. Nanotechnol. **5**, 251 (2010).

[6] Y. Zhang, M. S. Dresselhaus, Y. Shi, Z. Ren, and G. Chen, Nano Lett. **11**, 1166 (2011).

[7] A. A. Balandin, Nat. Mater. **10**, 569 (2011).

[8] A. M. Marconnet, M. A. Panzer, and K. E. Goodson, Rev. Mod. Phys. **85**, 1295 (2013).

[9] B. Wu, A. Heidelberg, and J. J. Boland, Nat. Mater. **4**, 525 (2005).

[10] C. Q. Chen, Y. Shi, Y. S. Zhang, J. Zhu, and Y. J. Yan, Phys. Rev. Lett. **96**, 075505 (2006).

[11] B. Wen, J. E. Sader, and J. J. Boland, Phys. Rev. Lett. **101**, 175502 (2008).

[12] M. F. L. De Volder, S. H. Tawfick, R. H. Baughman, and A. J. Hart, Science **339**, 535 (2013).

[13] D. Kauffman and A. Star, Angew. Chem., Int. Ed. **47**, 6550 (2008).

[14] Q. Cao and J. A. Rogers, Adv. Mater. **21**, 29 (2009).

[15] L. Liu, W. Ma, and Z. Zhang, Small **7**, 1504 (2011).

[16] W. Lu and C. M. Lieber, Nat. Mater. **6**, 841 (2007).

[17] Z. Fan, J. C. Ho, T. Takahashi, R. Yerushalmi, K. Takei, A. C. Ford, Y.-L. Chueh, and A. Javey, Adv. Mater. **21**, 3730 (2009).

[18] J. A. Rogers, T. Someya, and Y. Huang, Science **327**, 1603 (2010).

[19] H. Cebeci, I. Y. Stein, and B. L. Wardle, Appl. Phys. Lett. **104**, 023117 (2014).

[20] A. Striolo, A. A. Chialvo, K. E. Gubbins, and P. T. Cummings, J. Chem. Phys. **122**, 234712 (2005).

[21] J. A. Thomas and A. J. H. McGaughey, J. Chem. Phys. **128**, 084715 (2008).

[22] G. Cicero, J. C. Grossman, E. Schwegler, F. Gygi, and G. Galli, J. Am. Chem. Soc. **130**, 1871 (2008).

[23] C. Calero, M. C. Gordillo, and J. Marti, J. Chem. Phys. **138**, 214702 (2013).

[24] Y. Homma, S. Chiashi, T. Yamamoto, K. Kono, D. Matsumoto, J. Shitaba, and S. Sato, Phys. Rev. Lett. **110**, 157402 (2013).

[25] K. Nagatsu, S. Chiashi, S. Konabe, and Y. Homma, Phys. Rev. Lett. **105**, 157403 (2010).

[26] A. V. Krasheninnikov and K. Nordlund, J. Appl. Phys. **107**, 071301 (2010).

[27] J. G. Davis, B. M. Rankin, K. P. Gierszal, and D. Ben-Amotz, Nat. Chem. **5**, 796 (2013).

[28] V. V. Gobre and A. Tkatchenko, Nat. Commun. **4**, 2341 (2013).

[29] S. Han, M. Y. Choi, P. Kumar, and H. E. Stanley, Nat. Phys. **6**, 685 (2010).

[30] T. A. Pascal, W. A. Goddard, and Y. Jung, Proc. Natl. Acad. Sci. U. S. A. **108**, 11794 (2011).

[31] T. Ohba, H. Kanoh, and K. Kaneko, J. Phys. Chem. B **108**, 14964 (2004).

[32] M. Thommes, J. Morell, K. A. Cychosz, and M. Fröba, Langmuir **29**, 14893 (2013).

[33] T. Ohba, H. Kanoh, and K. Kaneko, J. Am. Chem. Soc. **126**, 1560 (2004).

[34] T. Kimura, H. Kanoh, T. Kanda, T. Ohkubo, Y. Hattori, Y. Higaonna, R. Denoyel, and K. Kaneko, J. Phys. Chem. B **108**, 14043 (2004).

[35] E. Bekyarova, Y. Hanzawa, K. Kaneko, J. Silvestre-Albero, A. Sepulveda-Escribano, F. Rodriguez-Reinoso, D. Kasuya, M. Yudasaka, and S. Iijima, Chem. Phys. Lett. **366**, 463 (2002).

[36] A. Alexiadis and S. Kassinos, Chem. Rev. **108**, 5014 (2008).

[37] H. Kumar, B. Mukherjee, S.-T. Lin, C. Dasgupta, A. K. Sood, and P. K. Maiti, J. Chem. Phys. **134**, 124105 (2011).

[38] H. Kyakuno, K. Matsuda, H. Yahiro, Y. Inami, T. Fukuoka, Y. Miyata, K. Yanagi, Y. Maniwa, H. Kataura, T. Saito, M. Yumura, and S. Iijima, J. Chem. Phys. **134**, 244501 (2011).

[39] P. Lazar, F. Karlick, P. Jureka, M. Kocman, E. Otyepkov, K. afov, and M. Otyepka, J. Am. Chem. Soc. **135**, 6372 (2013).

[40] X. Feng, S. Maier, and M. Salmeron, J. Am. Chem. Soc. **134**, 5662 (2012).

[41] C.-J. Shih, M. S. Strano, and D. Blankschtein, Nat. Mater. **12**, 866 (2013).

[42] H. Y. Yang, Z. J. Han, S. F. Yu, K. L. Pey, K. Ostrikov, and R. Karnik, Nat. Commun. **4**, 2200 (2013).

[43] Y. Ma, P. O. Lehtinen, A. S. Foster, and R. M. Nieminen, New J. Phys. **6**, 68 (2004).

[44] R. Singh and P. Kroll, J. Phys.: Condens. Matter **21**, 196002 (2009).

[45] G. Giambastiani, S. Cicchi, A. Giannasi, L. Luconi, A. Rossin, F. Mercuri, C. Bianchini, A. Brandi, M. Melucci, G. Ghini, P. Stagnaro, L. Conzatti, E. Passaglia, M. Zoppi, T. Montini, and P. Fornasiero, Chem. Mater. **23**, 1923 (2011).

[46] Z. He, H. Xia, X. Zhou, X. Yang, Y. Song, and T. Wang, J. Phys. D: Appl. Phys. **44**, 085001 (2011).

[47] M. R. Powell, L. Cleary, M. Davenport, K. J. Shea, and Z. S. Siwy, Nat. Nanotechnol. **6**, 798 (2011).

[48] R. Raj, S. C. Maroo, and E. N. Wang, Nano Lett. **13**, 1509 (2013).

[49] A. C. Ferrari and J. Robertson, Phys. Rev. B **61**, 14095 (2000).

[50] M. S. Dresselhaus, A. Jorio, M. Hofmann, G. Dresselhaus, and R. Saito, Nano Lett. **10**, 751 (2010).

[51] M. Bedewy and A. J. Hart, Nanoscale **5**, 2928 (2013).

[52] A. C. Ferrari and D. M. Basko, Nat. Nanotechnol. **8**, 235 (2013).

[53] S. Brunauer, P. H. Emmett, and E. Teller, J. Am. Chem. Soc. **60**, 309 (1938).

[54] M. Rahimi, J. K. Singh, D. J. Babu, J. J. Schneider, and F. Mller-Plathe, J. Phys. Chem. C **117**, 13492 (2013).

[55] I. Y. Stein and B. L. Wardle, Phys. Chem. Chem. Phys. **15**, 4033 (2013).

[56] A. J. Hart and A. H. Slocum, J. Phys. Chem. B **110**, 8250 (2006).

[57] I. Y. Stein and B. L. Wardle, Carbon **68**, 807 (2014).

[58] C. J. Van Oss, M. K. Chaudhury, and R. J. Good, Chem. Rev. **88**, 927 (1988).

[59] C. D. Latham, M. I. Heggie, M. Alatalo, S. Öberg, and P. R. Briddon, J. Phys.: Condens. Matter **25**, 135403 (2013).

[60] T. Trevethan, P. Dyulgerova, C. D. Latham, M. I. Heggie, C. R. Seabourne, A. J. Scott, P. R. Briddon, and M. J. Rayson, Phys. Rev. Lett. **111**, 095501 (2013).

[61] R. H. Telling, C. P. Ewels, A. A. El-Barbary, and M. I. Heggie, Nat. Mater. **2**, 333 (2003).

[62] C. Kamal, T. K. Ghanty, A. Banerjee, and A. Chakrabarti, J. Chem. Phys. **131**, 164708 (2009).

[63] A. J. Misquitta, J. Spencer, A. J. Stone, and A. Alavi, Phys. Rev. B **82**, 075312 (2010).

[64] M. M. Calbi, S. M. Gatica, D. Velegol, and M. W. Cole, Phys. Rev. A **67**, 033201 (2003).

[65] G. L. Klimchitskaya, U. Mohideen, and V. M. Mostepanenko, Rev. Mod. Phys. **81**, 1827 (2009).

[66] J. Zou, Z. Marcet, A. W. Rodriguez, M. T. H. Reid, A. P. McCauley, I. I. Kravchenko, T. Lu, Y. Bao, S. G. Johnson, and H. B. Chan, Nat. Commun. **4**, 1845 (2013).

[67] K. A. Milton, E. K. Abalo, P. Parashar, N. Pourtolami, I. Brevik, and S. r. Ellingsen, J. Phys. A: Math. Theor. **45**, 374006 (2012).

[68] H. B. G. Casimir, Proc. K. Ned. Akad. Wet. **51**, 793 (1948).

[69] I. Dzyaloshinskii, E. Lifshitz, and L. Pitaevskii, Advan. Phys. **10**, 165 (1961).

[70] F. C. Lombardo, F. D. Mazzitelli, P. I. Villar, and D. A. R. Dalvit, Phys. Rev. A **82**, 042509 (2010).

[71] M. Boström, B. E. Sernelius, G. Baldissera, C. Persson, and B. W. Ninham, Phys. Rev. A **85**, 044702 (2012).

[72] M. Boström, B. E. Sernelius, I. Brevik, and B. W. Ninham, Phys. Rev. A **85**, 010701 (2012).

[73] J. F. Dobson and T. Gould, J. Phys.: Condens. Matter **24**, 073201 (2012).

[74] G. Chen, D. N. Futaba, H. Kimura, S. Sakurai, M. Yumura, and K. Hata, *ACS Nano*, ACS Nano **7**, 10218 (2013).

[75] G. L. Klimchitskaya, E. V. Blagov, and V. M. Mostepanenko, J. Phys. A: Math. Theor. **41**, 164012 (2008).

[76] Z. Li, Y. Wang, A. Kozbial, G. Shenoy, F. Zhou, R. McGinley, P. Ireland, B. Morganstein, A. Kunkel, S. P. Surwade, L. Li, and H. Liu, Nat. Mater. **12**, 925 (2013).

[77] P. Cao, K. Xu, J. O. Varghese, and J. R. Heath, Nano Lett. **11**, 5581 (2011).

[78] K. Xu and J. R. Heath, Nat. Mater. **12**, 872 (2013).

[79] B. L. Wardle, D. S. Saito, E. J. García, A. J. Hart, R. Guzmán de Villoria, and E. A. Verploegen, Adv. Mater. **20**, 2707 (2008).

[80] H. Cebeci, R. Guzmán de Villoria, A. J. Hart, and B. L. Wardle, Compos. Sci. Technol. **69**, 2649 (2009).

[81] A. M. Marconnet, N. Yamamoto, M. A. Panzer, B. L. Wardle, and K. E. Goodson, ACS Nano **5**, 4818 (2011).

[82] D. Handlin, I. Y. Stein, R. Guzman de Villoria, H. Cebeci, E. M. Parsons, S. Socrate, S. Scotti, and B. L. Wardle, J. Appl. Phys. **114**, 224310 (2013).

[83] I. Y. Stein, *Synthesis and Characterization of Next-Generation Multifunctional Material Architectures: Aligned Carbon Nanotube Carbon Matrix Nanocom-*

posites, Master's thesis, Massachusetts Institute of Technology (2013).

[84] J. Köfinger, G. Hummer, and C. Dellago, Proc. Natl. Acad. Sci. U. S. A. **105**, 13218 (2008).

Supporting Information: Exohedral Physisorption of Ambient Moisture Scales Non-monotonically with Fiber Proximity in Aligned Carbon Nanotube Arrays

Itai Y. Stein

Department of Mechanical Engineering,

Massachusetts Institute of Technology,

77 Massachusetts Ave, Cambridge, MA 02139, USA.

Noa Lachman and Brian L. Wardle[*]

Department of Aeronautics and Astronautics,

Massachusetts Institute of Technology,

77 Massachusetts Ave, Cambridge, MA 02139, USA.

Mackenzie E. Devoe

Department of Materials Science and Engineering,

Massachusetts Institute of Technology,

77 Massachusetts Ave, Cambridge, MA 02139, USA.

[*] wardle@mit.edu.

I. PHYSISORPTION ON THE CNT SURFACE

Assuming negligible surface roughness, the specific surface area (SSA) of a CNT can be modeled using only the average CNT inner (D_i) and outer (D_o) diameters, and the the average CNT intrinsic density (ρ_{cnt}). Since the cross-sectional geometry of the CNTs (see Figure 2 in the main text) is simple and no adsorption between the CNT walls should occur, the SSA for a CNT with an inaccessible core (Ξ_e), where exohedral adsorption will occur, and a CNT with an accessible core(Ξ_u), where unrestricted adsorption will occur, can be modeled as follows:

$$\Xi_e = \left(\frac{4}{\rho_{cnt}D}\right) \tag{S1a}$$

$$\Xi_u = \frac{4}{\rho_{cnt}}\left(\frac{1}{D_o} + \frac{1}{D_i}\right) \tag{S1b}$$

Since the CNT arrays used here are comprised of a population of $3-7$ walled mulitwalled CNTs,[1] there may be an interest in calculating the SSA as a function of the number of walls (n) for both the exohedral ($\Xi_{u,n}$) and unrestricted cases ($\Xi_{u,n}$). This can be achieved by evaluating the outer diameter ($D_{o,n}$) and intrinsic CNT density ($\rho_{cnt,n}$) as a function of the number of walls using the van der Waals radius of carbon ($r_{vdW} \to \simeq 1.705$ Å) and the density of graphene ($\rho_g \to \simeq 2.25$ g/cm³)[2], leading to the following relations (D_i is assumed to remain constant):

$$\Xi_{e,n} = \left(\frac{4}{\rho_{cnt,n}D_{o,n}}\right) \tag{S2a}$$

$$\Xi_{u,n} = \frac{4}{\rho_{cnt,n}}\left(\frac{1}{D_{o,n}} + \frac{1}{D_i}\right) \tag{S2b}$$

$$\rho_{cnt,n} = 8\rho_g r_{vdW}\left(\frac{\sum_{j=1}^{n}(D_i + 4r_{vdw}(j-1))}{D_{o,n}^2}\right) \tag{S2c}$$

$$D_{o,n} = D_i + 4r_{vdw}(n-1) \tag{S2d}$$

See Table S1 for a table of the predicted SSA values for both exohedral and unrestricted adsorption for the CNTs used here.

Using the these relations, the SSA of CNTs determined using the BET analysis, or an equivalent method, can be used to non-destructively determine if the CNTs have an

TABLE S1. Model predicted and experimentally determined specific surface area for exohedral ($\Xi_{e,n}$) and unrestricted ($\Xi_{u,n}$) adsorption as a function of the CNT outer diameter ($D_{o,n}$), intrinsic density ($\rho_{cnt,n}$), and number of walls (n).

n	$D_{o,n}$ (nm)	$\rho_{cnt,n}$ (g/cm^3)	$\Xi_{e,n}$ (m^2/g)	$\Xi_{u,n}$ (m^2/g)
3	6.364	1.291	486.9	1106.5
4	7.046	1.489	381.4	918.9
5	7.728	1.634	316.7	806.2
5.4 ± 0.4[2]	~ 8[1]	~ 1.7[2]	–	776.8 ± 16.3[a]
6	8.410	1.745	272.6	731.1
7	9.092	1.830	240.4	677.5

[a] Experimental data.

accessible core. This would not be true if the highly destructive high resolution transmission electron microscopy was used instead.

II. THEORETICAL FRAMEWORK

This Section contains the equations used to compute the inter-CNT spacings, the thickness of the physisorbed water layer, and the accessible CNT array porosity.

A. Inter-CNT spacing relations

A previous study[3] developed the following relationship between the average inter-CNT spacing (Γ), the CNT volume fraction (V_f), the CNT outer diameter (D_o), and the two dimensional coordination number (N) of an idealized aligned CNT system (See Figure S1 for an illustration of the geometry):

$$\Gamma = D_\mathrm{o}\left((11.77(N)^{-3.042} + 0.9496)\sqrt{\frac{\sqrt{3}\pi}{6V_\mathrm{f}}} - 1\right) \tag{S3a}$$
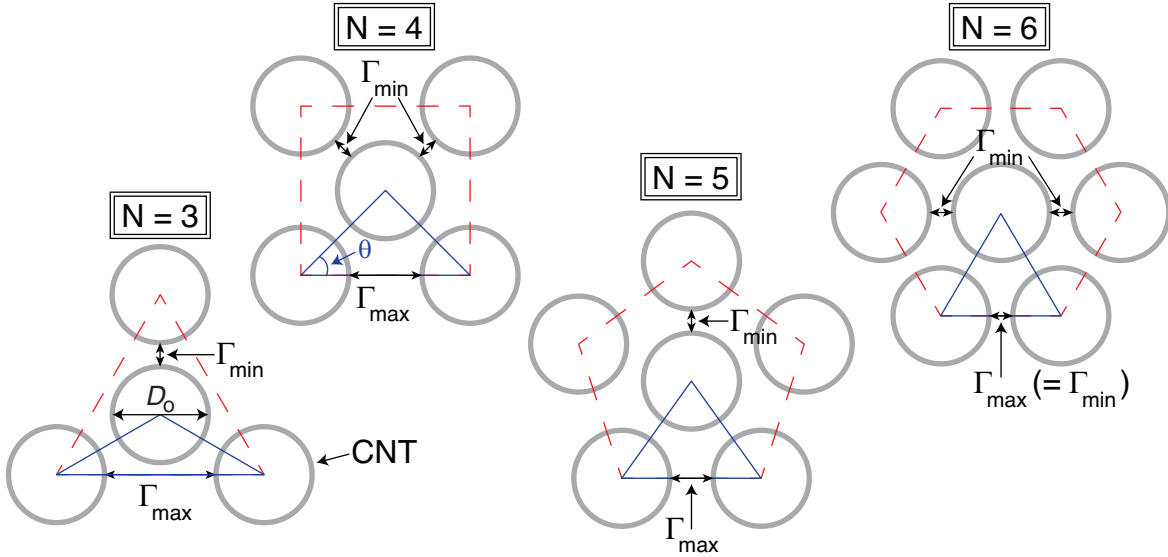
$$N = 2.511(V_\mathrm{f}) + 3.932 \tag{S3b}$$

FIG. S1. Illustration of the geometry used to derive the continuous coordination model.[3] The isosceles angle (θ) of the constitutive triangles at each coordination (N) is used to convert the previously reported[3] average inter-CNT spacing (Γ) into its two components, the minimum (Γ_min) and maximum (Γ_max) inter-CNT spacings.

Using the isosceles angle (θ) of the constitutive triangles at each N, the minimum ($\Gamma_{\min}$) and maximum ($\Gamma_{\max}$) inter-CNT spacings can be separated from Γ, yielding the following:

$$\theta = \pi \left(\frac{1}{2} - \frac{1}{N} \right) \tag{S4a}$$

$$\Gamma_{\min} = 2 \left(\frac{\Gamma}{1 + 2\cos(\theta)} \right) \tag{S4b}$$

$$\Gamma_{\max} = 4\cos(\theta) \left(\frac{\Gamma}{1 + 2\cos(\theta)} \right) \tag{S4c}$$

B. Water physisorption equations

For exohedral adsorption of water, the thickness of the water layer (w) can be found using the ratio of the wet (m_{wet}) and dry (m_{dry}) CNT array mass, defined as $m^{\star}$, the cross-sectional area of the CNTs (A_{cnt}), defined using the inner ($D_{\text{i}} \rightarrow \simeq 5$ nm)[1] and outer ($D_{\text{o}} \rightarrow \simeq 8$ nm)[1] diameters of the CNTs, the ratio of the CNT intrinsic density ($\rho_{\text{cnt}} \rightarrow \simeq 1.7$ g/cm^3)[2] and the average density of the water layer (ρ_{w}), and the equilibrium separation of the water molecules and the CNT wall ($\ell \rightarrow \simeq 0.3$ nm)[4]. The equation takes the following form:

$$w = \left(\sqrt{\frac{4A_{\text{cnt}}}{\pi} \left(\frac{\rho_{\text{cnt}}}{\rho_{\text{w}}} (m^{\star} - 1) \right) - D_{\text{i}}^2} \right) - D_{\text{o}} + \ell \tag{S5a}$$

$$A_{\text{cnt}} = \frac{\pi}{4}(D_{\text{o}}^2 - D_{\text{i}}^2) \tag{S5b}$$

$$m^{\star} = \frac{m_{\text{wet}}}{m_{\text{dry}}} \tag{S5c}$$

To evaluate eq S5, ρ_{w} needs to be evaluated at its current thickness. While the results of a previously reported molecular dynamics simulation illustrated that ρ_{w} can vary noticeably from the bulk value (~ 1.0 g/cm^3) at $w \lesssim 1$ nm (see Table S2),[4] since w is significantly greater than 1 nm here, the bulk value for the water layer density was used throughout the calculations.

TABLE S2. Average densities of the physisorbed water layer (ρ_w) evaluated at different water layer thicknesses (w) using the results of a previously reported molecular dynamics simulation[4].

w (nm)	0.1	0.2	0.3	0.4	0.5	0.6	0.7	0.8	0.9	1.0
ρ_w (g/cm^3)	1.12	0.996	0.946	0.957	0.980	0.988	0.987	0.987	0.989	0.991

III.   WATER PHYSISORPTION AS A FUNCTION OF CNT PACKING

This Section contains the experimental data, and the scaling equations for both Mode I and Mode II from the main text.

A.   Experimental results

TABLE S3. Experimentally determined ratios of the wet and dry CNT array mass ($m^\star$) for CNT volume fractions (V_f) up to 20%, and the evaluated values of the water layer thickness (w) and the accessible porosity (ϕ) estimated using both $m^\star$ (ϕ_{mass}) and the matrix porosity of A-CNT carbon matrix nanocomposites ($\phi_{infusion}$).

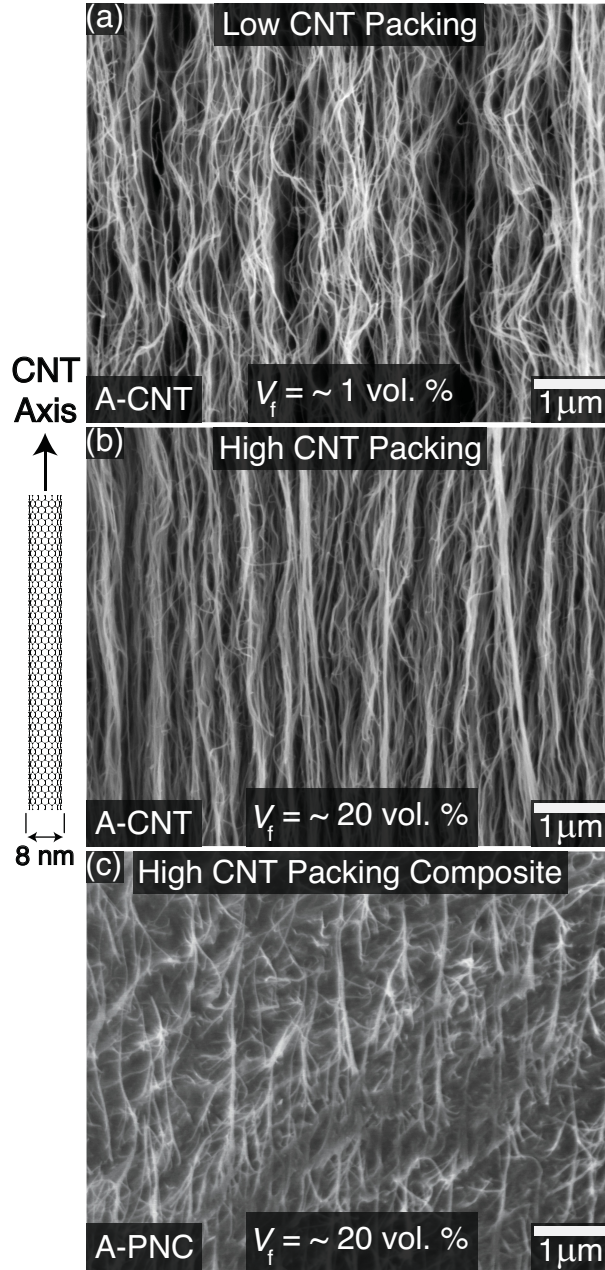| V_f (%)	$m^\star$	w (nm)	ϕ_{mass} (%)	$\phi_{infusion}$ (%)
1	2.14 ± 0.18	3.50 ± 0.50	96.5 ± 0.5	94.0 ± 4.0
5	3.34 ± 0.45	6.50 ± 0.90	65.5 ± 6.0	54.7 ± 8.0
10	2.91 ± 0.13	5.50 ± 0.30	43.5 ± 3.5	43.8 ± 2.5
20	2.48 ± 0.08	4.40 ± 0.15	11.7 ± 3.2	13.1 ± 1.0

FIG. S2. High resolution scanning electron microscopy images of the cross-sectional morphology of A-CNT forests (a and b) and a polymer composite (c) of $V_f \sim 1\%$ (a) and $V_f \sim 20\%$ (b and c) illustrating continuous through thickness infusion with polymer. Once heat treated, the density of the pyrolytic carbon matrix was used to estimate the accessible A-CNT array porosity, and can be found in Figure 3b in the main text.
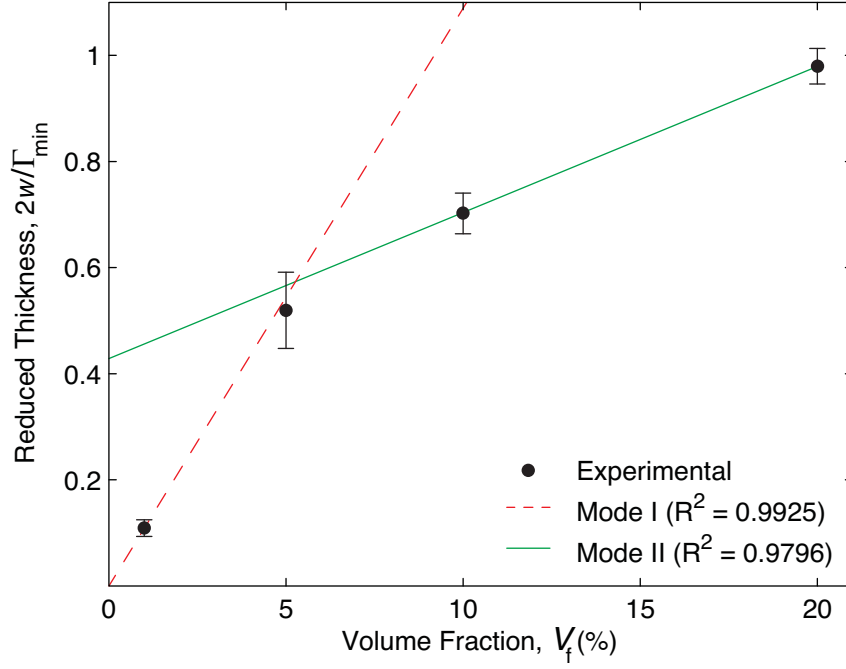
B. Scaling behavior

FIG. S3. Plot of the reduced water layer thickness $(2w/\Gamma_{\min})$ vs. CNT volume fraction (V_{f}) illustrating the transition from Mode I $(R^2 = 0.9925)$ to Mode II $(R^2 = 0.9796)$ at $V_{\mathrm{f}} \sim 5.3\%$. The equations for the two modes are evaluated by fitting straight lines through each regime $(V_{\mathrm{f}} \lesssim 5\%$ and $V_{\mathrm{f}} \gtrsim 5\%)$, yielding $V_{\mathrm{f}} = 0.1089(2w/\Gamma_{\min})$ $(R^2 = 0.9925)$ for Mode I, and $V_{\mathrm{f}} = 0.02752(2w/\Gamma_{\min}) + 0.4286$ $(R^2 = 0.9796)$ for Mode II. Solving for the crossover point of the two modes yields $V_{\mathrm{f}} \sim 5.3\%$.

[1] A. J. Hart and A. H. Slocum, J. Phys. Chem. B **110**, 8250 (2006).

[2] I. Y. Stein and B. L. Wardle, Carbon **68**, 807 (2014).

[3] I. Y. Stein and B. L. Wardle, Phys. Chem. Chem. Phys. **15**, 4033 (2013).

[4] J. A. Thomas and A. J. H. McGaughey, J. Chem. Phys. **128**, 084715 (2008).